PERGAMON

Journal of Structural Geology 21 (1999) 1351–1368

JOURNAL OF STRUCTURAL GEOLOGY

www.elsevier.nl/locate/jstrugeo

Effects of lithology on geometry and scaling of small faults in Triassic sandstones, East Greenland

Øyvind Steen* [1], Arild Andresen

Department of Geology, University of Oslo, P.O. Box 1047 Blindern, 0316 Oslo, Norway

Received 5 May 1998; accepted 27 April 1999

Abstract

A study of the Lower Triassic sandstones exposed in the Månedalen Fault Zone on Traill Ö, East Greenland, reveals how diagenetic carbonate cement affects the deformational behaviour of sandstones. A siliciclastic sequence of beds ($\simeq$300 m thick) is variably cemented because of the precipitation of carbonate close to stromatolitic interbeds. Displacements or throws of minor faults (<1.8 m) were sampled along lines through damage zones of major faults (throws >9 m) in three different lithologies: (1) Porous sandstones with little carbonate cement, (2) low-porosity sandstones rich in carbonate cement, and (3) thin beds of carbonate-cemented sandstone in mudstone. The latter shows a strong anisotropy causing fault refraction with syn-kinematic calcite growth in the sandstone beds.

Viewed in a microscope, porous sandstones show disaggregated zones with porosity reduced by 40–60%, and cataclastic bands. The development of groups of cataclastic bands was governed by strain-hardening. The low-porous sandstones show cataclastic bands with minor textural change towards the bands. The apparent strength of these sandstones suggests that strain-hardening was much less significant for the development of the faults. Logarithmic plots of N vs D, where N is the cumulative number of faults with throw greater or equal to D, appear to follow linear trends. The least-square regression method gives the following values for the power-law exponent; $C = 1.01$ for 993 faults in the porous sandstones, $C = 0.70$ for 457 faults in carbonate-cemented sandstones, and $C = 0.38$ for 166 faults in the carbonate-cemented sandstones interbedded with mudstones. The estimated confidence intervals for C indicate a true difference in scaling relationships of the samples. The different scaling relationships cannot be linked to strain differences encountered along the traverses. Thus, the lithological heterogeneity arising from local calcite precipitation is thought to be the cause for the differences in deformational style and scaling behaviour.

1. Introduction

Self-similarity in fault systems has gained much attention in recent years (Barton and La Pointe, 1995; Cowie et al., 1996). Geometrical similarity leads to a power-law scaling of the size-frequency of faults. A commonly used power-law distribution is the *cumulative distribution function* which is expressed as

$$N = aD^{-C} \tag{1}$$

where N is the cumulative number of faults greater or equal to D, D is the size of the fault, a is a constant, and C is the power-law exponent (e.g. Walsh et al., 1991; Needham et al., 1996). On a $\log N$ vs $\log D$ graph this function will define a straight line with a slope of $-C$. A main problem in documenting fractal fault systems is the limited size of samples and the limited range in fault sizes obtained by any observational technique (Pickering et al., 1995; Nicol et al., 1996). Although the self-similarity of fault systems is observed at a particular scale, there may be geological factors which contribute to changes or breaks in scaling properties. Cowie and Scholz (1992) questioned the validity of combining data from different lithologies and tectonic settings because fault growth may depend

* Corresponding author.
E-mail address: oysteen@statoil.com (&.O. Steen)
[1] Present address: Statoil's Research Centre, Arkitekt Ebbels veg 10, Rotvoll, N-7005 Trondheim, Norway.

0191-8141/99/$ - see front matter
PII: S0191-8141(99)00100-5

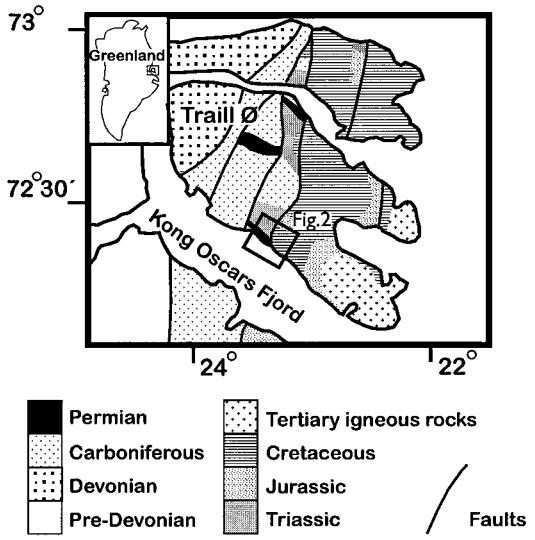

Fig. 1. Geological map of Traill Ö and adjacent areas. Location of Fig. 2 is shown on the map.

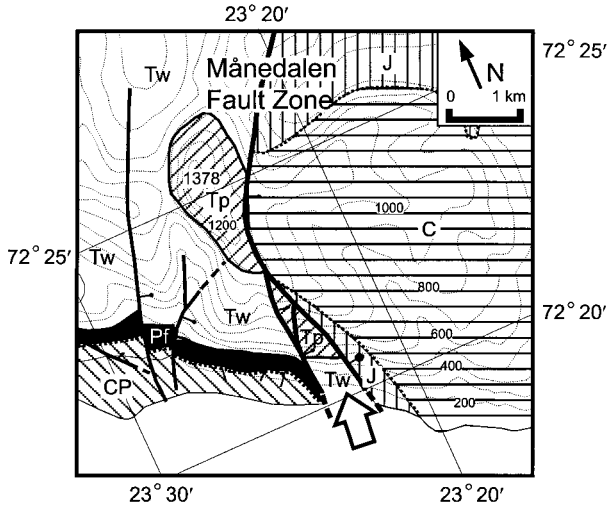

Fig. 2. Topographic map showing the location of Månedalen Fault Zone and other normal faults in its footwall (solid lines with dots on the downthrown side). The peak at 1378 m.a.s.l. is the Svinhufvuds Bjerge. Solid lines are conformable contacts between formations and dotted lines are unconformities. CP: Carboniferous–Permian, undifferentiated (right-dipping stripes). Pf: Upper Permian Foldvik Creek Formation (black). Tw: Lower Triassic Wordie Creek Formation (transparent). Tp: Middle Triassic Pingo Dal Formation (left-dipping stripes). J: Jurassic (vertical stripes). C: Cretaceous (horizontal stripes). The subdivision of the Triassic rocks is made by Clemmensen (1980b). The location of the photographer behind Fig. 3 is at the arrow point.

on material properties and loading conditions. Recently, Gross et al. (1997) showed that local lithological heterogeneities contribute to a wide scatter of length–displacement ratios of faults. Factors related to a dynamic growth of a fault system may also be responsible for breaks in scaling behaviour. Field observations by Wojtal (1996) demonstrated that changes in structural style during the temporal evolution of a fault system can cause different displacement population coefficients for faults of different sizes.

Effects of lithology on fault geometries can be observed on different scales. Outcrop studies show that fault refraction occurs in anisotropic rocks (e.g. Peacock and Sanderson, 1992). On a small scale, the appearance of microstructural features will depend on the main deformation mechanisms (Lucas and Moore, 1986; Antonellini et al., 1994). Shear zones and disorganized grain structures can be produced by grains moving past each other (independent particulate flow) (Lucas and Moore, 1986). Fractured grains, on the other hand, are produced by cataclastic mechanisms (Knipe, 1989). In sedimentary basins, sandstones can deform by independent particulate flow to depth of 2–4 km unless early cementation takes place by the dissolution and precipitation of biogenic silica or carbonate (Sverdrup and Bjørlykke, 1997). Early carbonate cement can lithify loose sand and cause spatial variations of the geomechanical properties in a siliciclastic sequence of beds (Bjørlykke and Høeg, 1997).

In this outcrop study, we describe faults which cut a heterogeneous sequence of siliciclastic rocks. The rocks appear to have been carbonate-cemented at different times during the tectonic history. By studying the microstructures and determining the timing of deformation relative to carbonate cementation, we document the main deformation mechanisms that have taken place in these lithologies. In light of these observations, we discuss possible links between lithology, deformation styles and populations of small fault displacements.

2. Geology of the study area

2.1. Geological setting

The study area is situated in the Månedalen Fault Zone on the southern coast of Traill Ö, East Greenland, where a Devonian–Cretaceous succession crops out. The sequence is intruded by Tertiary dolerite sills and dykes as well as syenitic plutons. The Månedalen Fault Zone is one of several major NNW-trending normal faults which bound the westerly rotated blocks in the Traill Ö region (Fig. 1). These fault blocks are cut by minor normal faults which offset the Early Tertiary dolerite sills. The magmatism and the later tectonism were associated with the final break-up of Pangea and the onset of sea-floor spreading in the Greenland Sea (Upton et al., 1995). The Månedalen Fault Zone probably initiated during Upper Carboniferous to Permian times and played a major role during the sediment deposition throughout

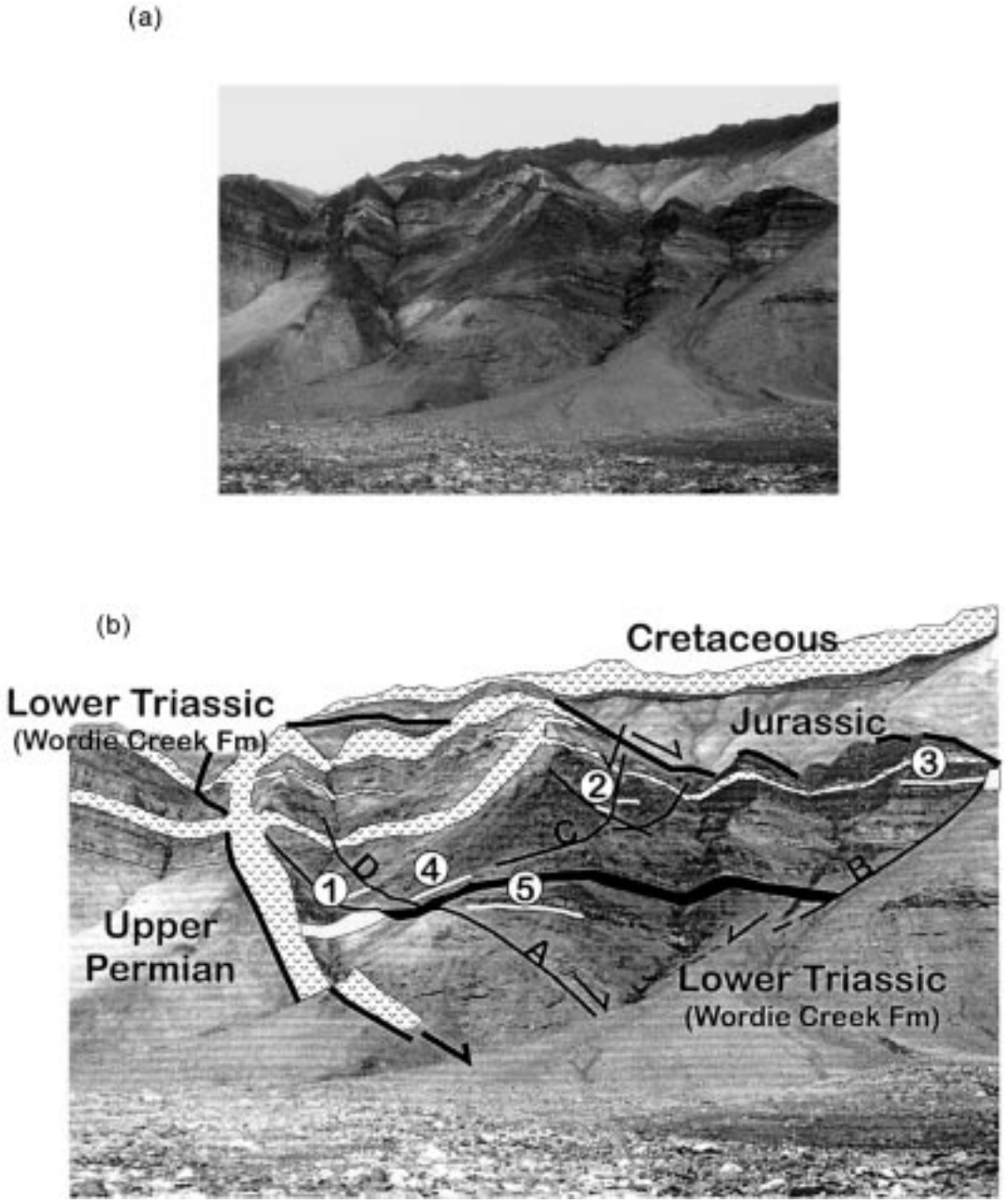

Fig. 3. (a) Photograph of the study area (the direction of view and location of photographer are indicated on Fig. 2). (b) Line-drawing on the photograph in (a). Polygons with v-hatches are diabase dykes and sills. Polygons with dots represent a conglomeratic sandstone unit, and the black area represents a stromatolitic reef unit. The line samples presented in the paper are shown by white lines (see the stratigraphic position of sedimentary units and line samples on Fig. 4a). The arrows show the sense of displacements along faults. There is no offset of the Tertiary dikes and sills except for some minor reactivation (<20 m) along the two largest faults (Fault A and B) with total throws of 130 and 190 m, respectively. Bedding dips from 0 to 15° east in the cliff section. The height difference between the photographer and line sample 2 is $\simeq$350 m.

Mesozoic times (Clemmensen, 1980a; Surlyk et al., 1981).

In the study area, a Lower Triassic succession occurs between two faults of the Månedalen Fault Zone (Fig. 2). This fault splay crops out in a cliff section about 1000 m high and extends for 2 km horizontal distance from the fjord and northwards to Svinhufvuds Bjerge (Fig. 2). Vertical separation across the two splays is calculated to be $\simeq$700 m and a minimum of 1000 m, respectively. The fault zone is intruded by Tertiary dolerite dikes and sills (Fig. 3). The offset of dikes across the fault zone indicates a phase of post-magmatic reactivation along the eastern fault of $\simeq$200 m vertical separation and minor reactivation along the western fault. Evidence of syn- to post-magmatic fault activity is rare between the fault splays but is common away from the fault block. A likely explanation for the local preservation of pre-magmatic fault offsets would

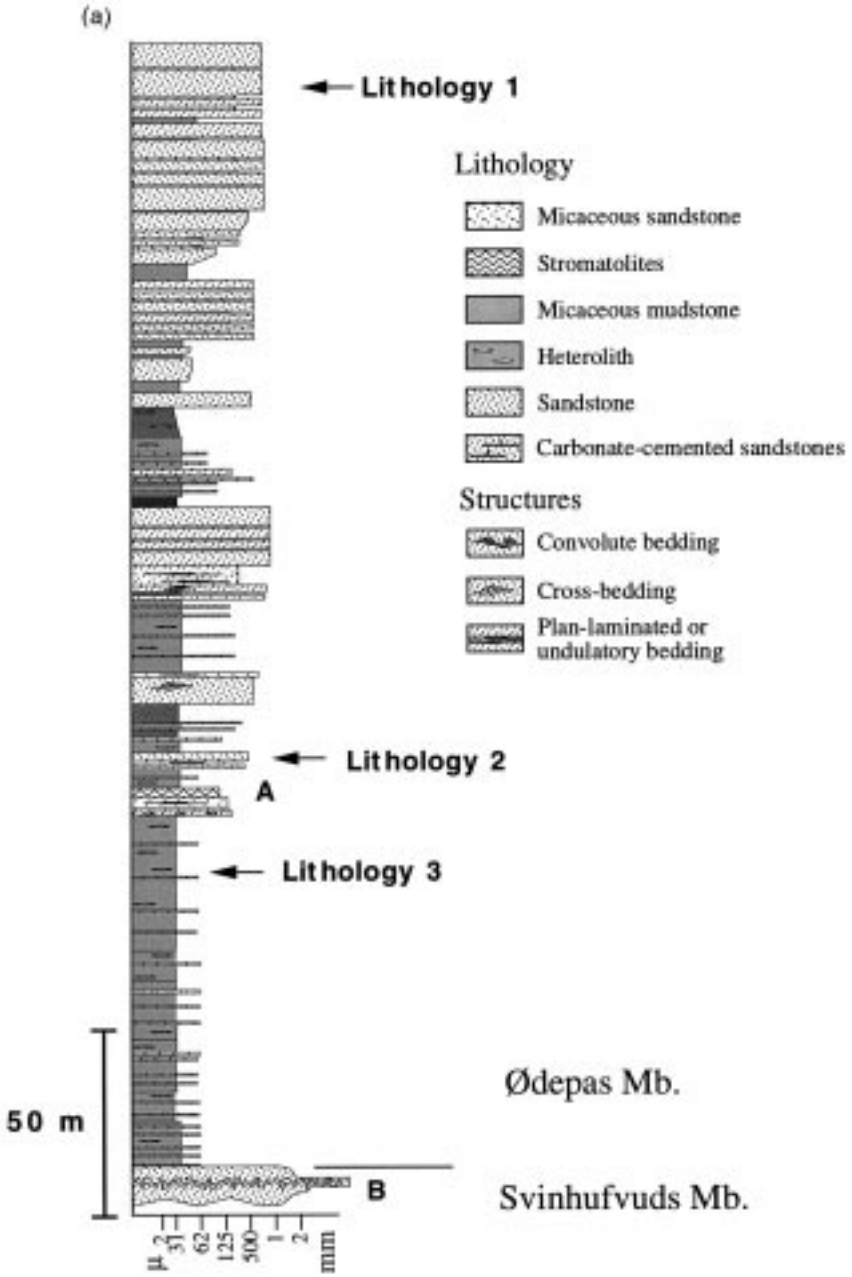

Fig. 4. (a) Stratigraphic log of the studied section including the upper part of the Svinhufvuds Bjerge Member and the Ødepas Member. Stratigraphic nomenclature from Clemmensen (1980b). Arrows show the stratigraphic position of the traverses for data collection. Lithology 1 = Sandstones with porosity 10% with cements composed of iron oxides, authigenic clay and minor carbonate. Lithology 2 = Sandstones with low porosity (<4%) with carbonate cement and minor authigenic clay. Lithology 3 = Carbonate-cemented sandstone interbedded with mudstone. The position of a stromatolitic reef unit is marked A (black polygon on Fig. 3) and the conglomeratic sandstone unit marked B (dotted polygon on Fig. 3). Transects 1, 2, and 3 on Fig. 3 are located in lithology 1, transect 4 in lithology 2, and transect 5 in lithology 3. (b) Kamb contour plot of poles to minor faults. Number of faults is 798. The Kamb contour interval was 4 sigma. (c) Histogram of pitch values measured on 189 conjugate faults with throws <2 m. Histogram intervals are 5°. The pitch is determined by the right-hand rule and varies from 0 to 180°. Data are shown for the two parts of the conjugate set (cf. b). Fifty-six per cent of all faults show dip-slip (pitch between 80° and 100°) and the rest show oblique-slip (pitch between 45° and 80° and between 100° and 130°).

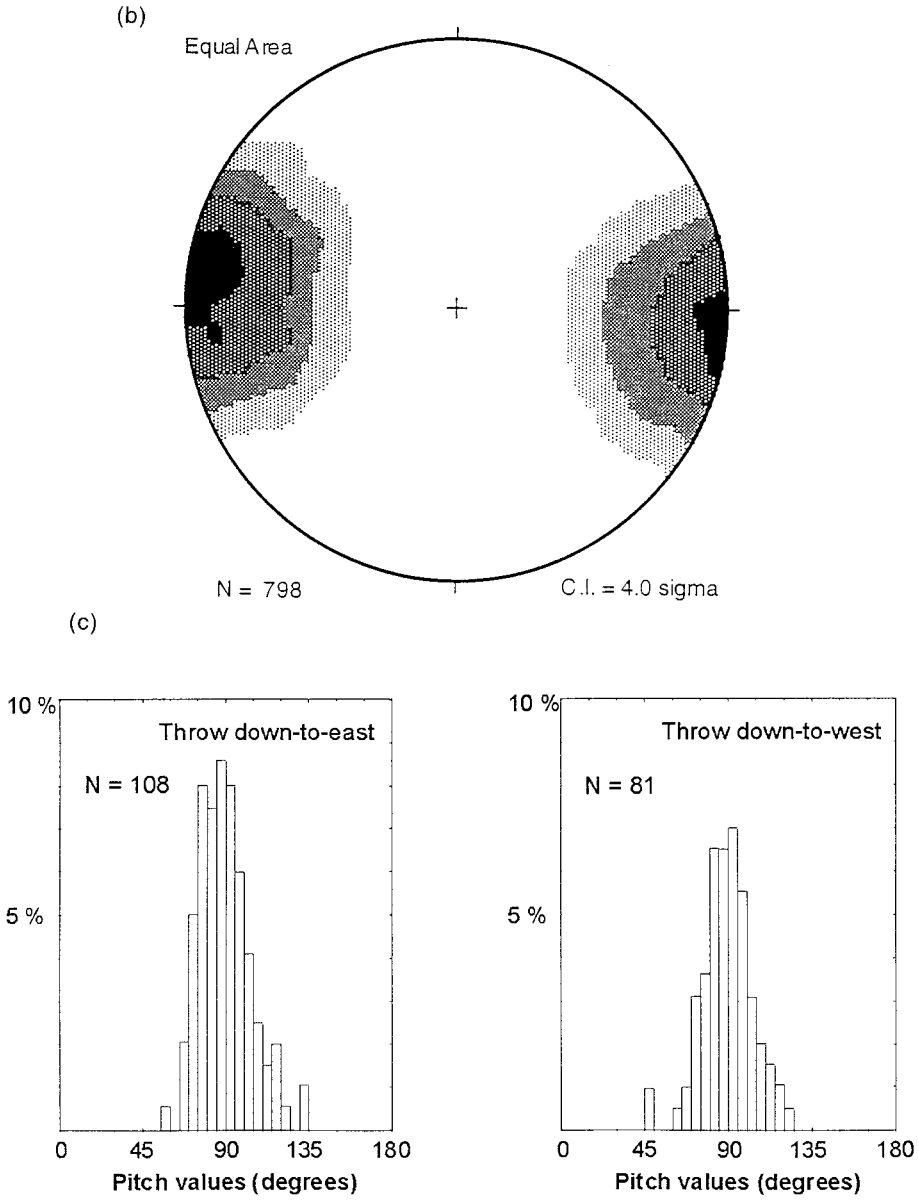

Fig. 4. (*continued*).

be that dike emplacement along the fault allowed for a change in fault rock properties so that the potential for fault reactivation was reduced. The unconformity between the Jurassic and Cretaceous deposits probably represents a late Jurassic to Early Cretaceous fault scarp (Surlyk, 1991; Price and Whitham, 1997). Syn-sedimentary faults are not found within the Triassic record on Traill Ö suggesting that the faults described in this paper were formed in Early Jurassic–Early Tertiary times before the dike intrusion.

2.2. Lithologies studied in detail

Sedimentary rocks in the study area are within the Ødepas Member which belongs to the Wordie Creek Formation (cf. Clemmensen, 1980b). This member is dominated by micaceous siltstones and fine-grained sandstones which grade into thicker sandstone units at the top (Fig. 4a). This study examines three rock types which mainly differ with respect to sandstone thickness, cement mineralogy, and porosity. The samples were vacuum-filled by epoxy before the preparation of thin-sections. Porosity values and the percentage mineral content listed below are obtained by using the point-counting technique in thin-sections.

Porous sandstones: The uppermost Ødepas Member and overlying rocks are dominated by cross-bedded, fine-to-medium grained sandstones. The sandstone beds are between 2 and 4 m thick and separate thin layers of mica-rich and fine-grained sandstones. In the

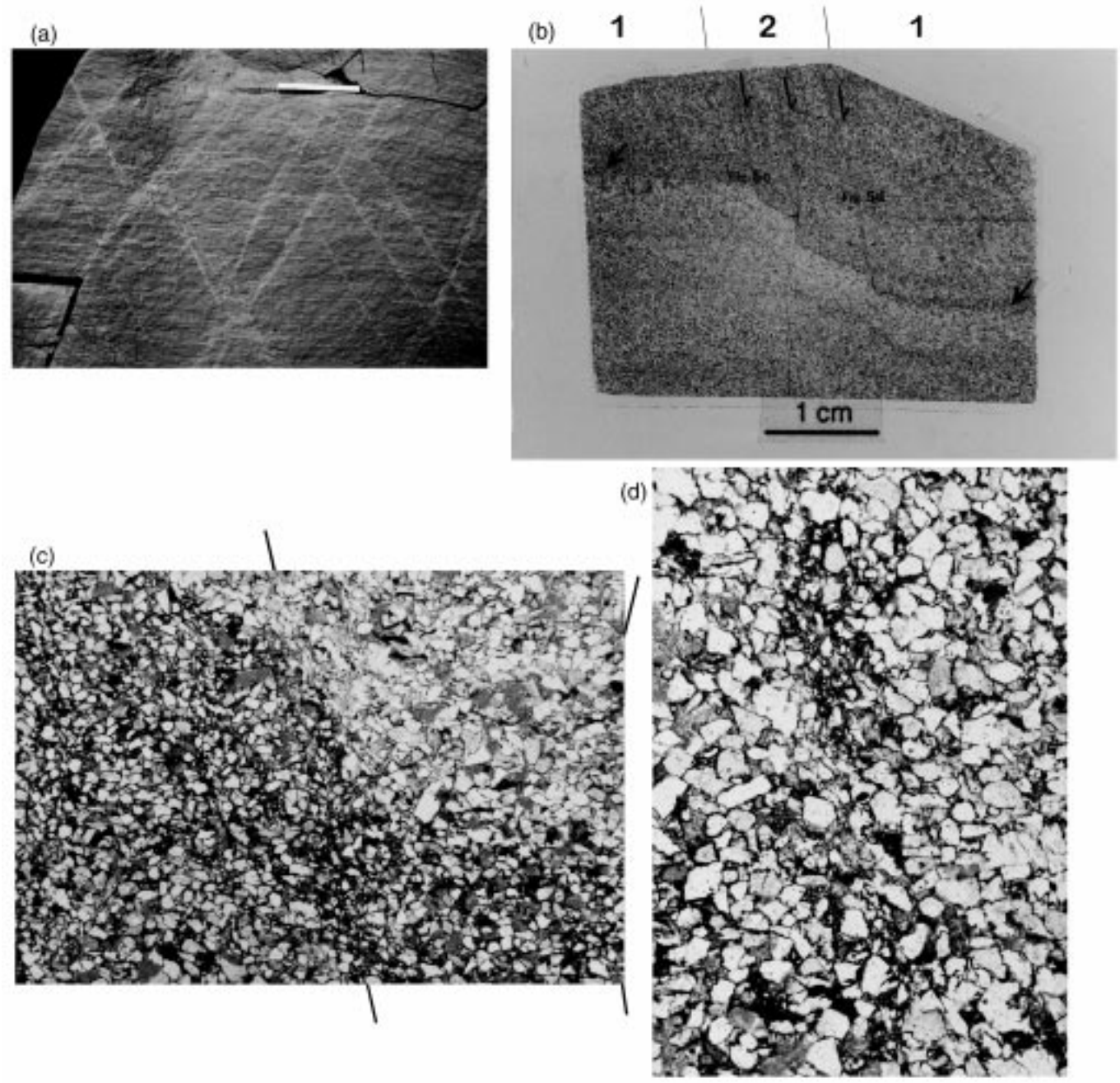

Fig. 5. (a–d) Outcrop and microstructural geometries of faults cutting the porous sandstones. (a) Conjugate set of deformation bands in porous sandstones. The bands occur individually or form groups of bands. The scale bar is 0.2 m long. (b) Photomicrograph of faults in a porous sandstone. The strike and dip of the section are 300° and 90°. Porosity in the undeformed sandstone on the picture is ≃35% (pore spaces were filled by green epoxy). Carbonate cement makes up ≃8% of the rock. Displacement patterns are indicated by laminae surfaces (full arrows point to the same surface). The fault zone shows rotated laminae surfaces and cataclastic bands (their sense of movement is indicated by half arrows). Locations of (c) and (d) are shown. See text for description and interpretation. 1: Undeformed sandstone. 2: Compacted sandstone with rotated laminae surfaces and cataclastic bands. (c) Picture of the same thin section as in (b) to illustrate the grain texture at the boundary between compacted sandstone and less compacted sandstone. Cataclastic zones are marked by solid lines. Laminae surfaces are rotated between the cataclastic bands. Around the cataclastic zones there is little evidence of fractures within the grains. The width of the picture is 6.5 mm. (d) Close-up picture of a cataclastic zone in (b). The zone shows fragmented grains of mainly feldspar and quartz. Porosity is less than 3% in the zone. The width of the picture is 3.25 mm.

microscope, the sandstones appear isotropic because of the good sorting and the high content of equidimensional grains (Fig. 5). Porosity ranges from 10 to 35%. The cement types are iron oxide and microcrystalline quartz coated on grains, authigenic clay minerals (mainly kaolinite), and blocky carbonate (<6%) in pore spaces.

Sandstones with low porosity: A 4.5 m thick sandstone bed a few metres above a stromatolite-bearing unit was examined. The bed is well exposed in a traverse starting 15 m away from Fault A and eastwards below Fault B. Carbonate cement constitutes 20–30% of this sandstone and the porosity is <4%, approaching zero in some samples. Matrix is made up mostly by calcite cement, and with minor authigenic clay.

Thinly bedded sandstones and siltstones: The lower part of the Ødepas Member consists of finely laminated sandstone and micaceous mudstone with some sandstone interbeds (<200 mm thick). This sequence occurs in the lower part of the cliff section between the two major conjugate faults (Faults A and B on Fig. 3). These sandstones contain various amounts of calcite cement which precipitated before the tectonic deformation. Fine-grained sandstones dominated by quartz and felspar grains contain up to 60% calcite cement with porosities <2%, whereas the interbedded mica-rich siltstones show 5–15% calcite cement.

2.3. Fault and fracture geometries

Accessible parts of the cliff-section show conjugate faults of variable intensity. The two largest faults are conjugate and show 130 and 190 m throw, respectively (Faults A and B on Fig. 3). Faults C and D with 60 and 9 m throw, respectively, occur in the hanging wall of these faults (Fig. 3). Fault C intersects the thick sandstone units at a steep angle ($\simeq 70^\circ$ dip) and flattens within the mudstone-dominated units to 20–30° dip. Mudstone beds are rotated to parallelism with this fault, and evidence of bedding parallel slip is abundant within these lithologies. Fault D is a synthetic fault to Fault A, which merge when going down the hill. Lineations along major faults (here defined as individual or linked faults which cut through the whole study section) pitch between 44 and 117°, but the majority of them indicate dip-slip movements within a few degrees. Faults with throws <1 m locally show syn-kinematic growth of calcite grains and striations in the siltstone wall rocks. All observations indicate that the small faults have a major component of normal slip (Figs. 4b and c). They occur in conjugate sets which dip commonly in the range between 50 and 80°. The following sections describe the geometry of small faults (throws <0.2 m), which are observed in the different rock types.

Porous sandstones: Mesoscopically, brittle deformation of the porous sandstones has taken place along numerous thin zones, which on weathered surfaces are light-coloured compared with the undeformed rock (Fig. 5a). The beds show minimal grading but lamina surfaces are abundant in the upper part of the beds and show evidence of millimetric fault displacements. These zones are shear fractures analogous to deformation bands (e.g. Aydin and Johnson, 1983; Antonellini et al., 1994; Antonellini and Aydin, 1995) and microfaults (Jamison and Stearns, 1982) in faulted sandstones.

Microstructural deformation associated with the shear fractures includes cataclasis and frictional grain-boundary sliding (Knipe, 1989) (Figs. 5b–d). Grain-boundary sliding appears to have produced domains with deflected lamina surfaces and disaggregated zones. Individual grains in such domains are mostly unfractured and elongated grains show local preferred orientation subparallel to the shear band. The carbonate cement precipitated after the fault deformation, as indicated by the unstrained carbonate between grains which have moved past each other. Domains with inferred grain boundary sliding occur in a few-millimetre wide zone around the cataclastic bands, which are relatively narrow (<2 mm). Scanning electron microscope (SEM) analysis of the centre of such zones shows angular grains (<0.01 mm) of mostly felspar, iron and titanium oxides, and minor quartz. Displacements along individual deformation bands are of the order of 1–4 mm, but additional displacements have commonly taken place by the disaggregation and folding of laminae (Fig. 5b). Displacements of 10 mm are typically accommodated by several bands which are subplanar and roughly subparallel with each other. In densely faulted areas, individual bands are closely associated with zones of bands and the interlinkage points between bands are frequent.

A three-fold division of small faults has been proposed by Aydin and Johnson (1978) and Underhill and Woodcock (1987); (1) an inner zone of highly fractured and poorly sorted grains, (2) an outer zone of moderately fractured grains with good sorting, and (3) undeformed parent rock. A similar subdivision may be adequate for some of the individual faults with a few millimetres displacement, although the dominant deformation mechanisms are different compared to faults studied by the above-mentioned authors. The inner part of the fault zone is equivalent to the mesoscopically visible bands and shows products from grain breakage and communition. Between the crushed zone and the undeformed parent rock there is commonly a zone of drag-folded or distorted lamina surfaces (Figs. 5b–d). Individual grains in this zone are not fractured and deformation has taken place by grain boundary sliding. Point counting of pore spaces indicates that the porosity has decreased from 20–35%

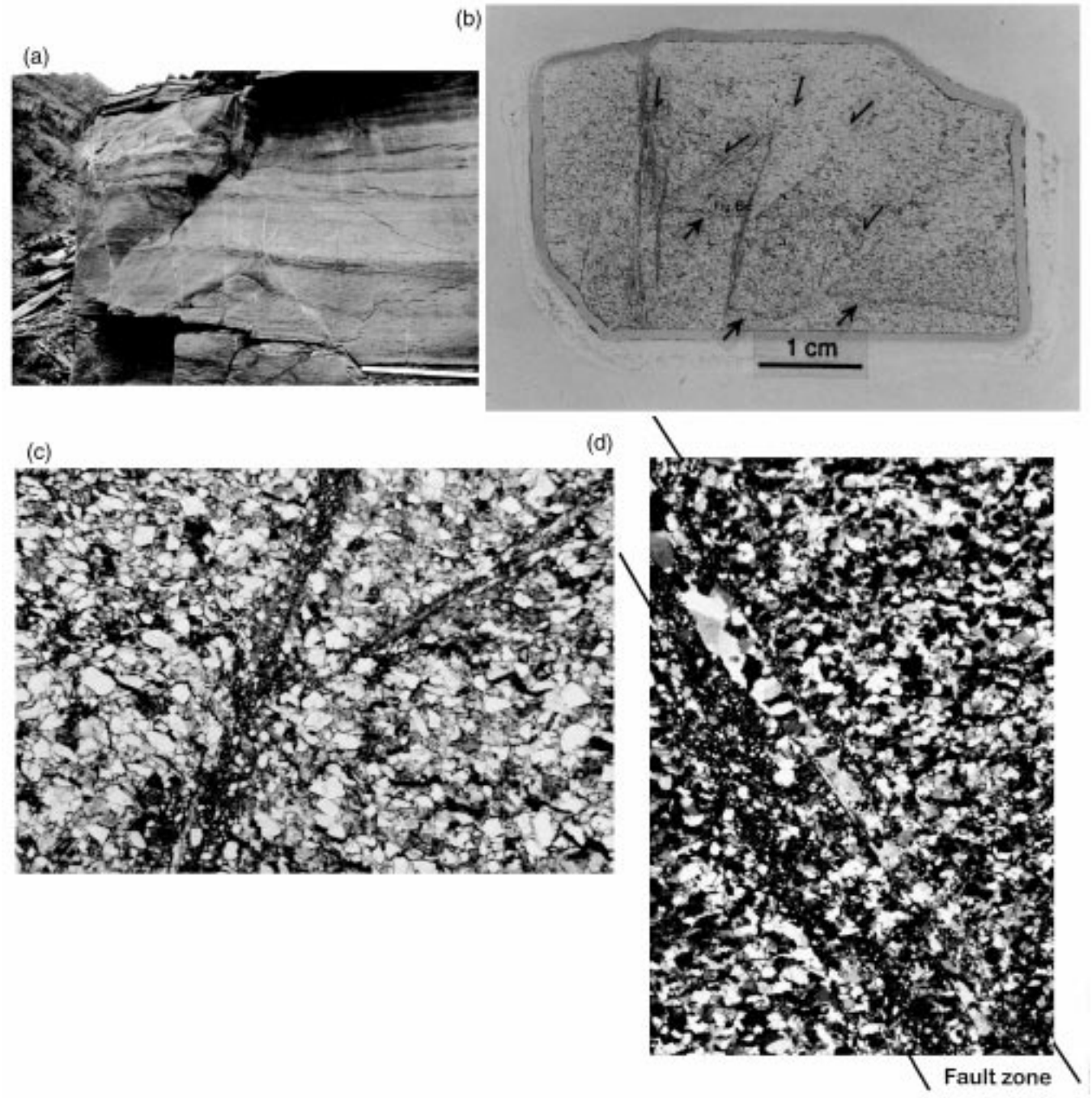

Fig. 6. (a–d) Outcrop and microstructural geometries of faults cutting the low-porosity and carbonate-cemented sandstone bed. (a) Conjugate faults occuring at the end of a line sample. The light-coloured bands are slightly undulating and form lenses of undeformed sandstone. The scale bar is 0.4 m long. (b) Photomicrograph of conjugate and cross-cutting faults. The strike and dip of the section are 265° and 90°. Porosity is <4% and carbonate cement constitutes ≃20% of the rock. Pore or fracture spaces are shown by the green epoxy. A lamina surface (marked by full arrows) can be traced across two faults (sense of movement along the faults are shown by half arrows). The frame of (c) is shown. (c) Photomicrograph of two conjugate faults in the thin-section. There is a sharp boundary between the undeformed host sandstone and the cataclastic zones. Grains in the zones are poorly sorted and their size is commonly very reduced compared to the grains outside the zones. The width of the picture is 6.5 mm (see location in b). (d) A photomicrograph (crossed nicols) of a fault zone in the same bed as shown in (a). The fault zone shows growth of blocky calcite cement along fracture planes. Shear fractures cutting through the calcite cement indicate a renewed movement along the fault zone after cement filling. The height of the picture is 6.5 mm.

in the undeformed rock to 10–15% in the disaggregated zone; a porosity reduction of 40–60%. The zones with folded laminae surfaces have variable thickness, ranging from almost zero to 5 mm along individual faults, and are commonly observed at the end of crushed zones and at fault oversteps. Fault zones with larger displacements commonly show several thin zones of crushed grains with drag-folded laminae surfaces in between. Rotated laminae are generally evident throughout the fault zone, even if crushed zones are spaced as far as 10 mm apart.

Zones of deformation bands with associated drag-folded laminae commonly show displacements <0.2 m and have shear strain values ranging from 0.4 to 3.8. Larger displacements are recorded along slip surfaces. Slip surfaces are roughly planar at the outcrop scale and show well defined striations. Displacements along the individual slip planes are commonly in the order of some decimetres, occasionally of several metres. The major faults typically have a fault zone consisting of a fault gouge and several slip surfaces. Along some parts of the slip surfaces, the growth of calcite fibres indicate that the slip surfaces may have acted as conduits for fluids at some time during deformation.

Sandstones with low porosity: Deformation bands in this rock have a light appearance relative to the greenish to greyish weathered surface of the host rock. They are 1–3 mm thick and show displacements commonly of the order of several millimetres, occasionally up to 50 mm. The mesoscopic geometry of the deformation bands differs from those cutting the more porous sandstones by the wavy and curved geometries, and the common occurrence of solitary bands (Fig. 6a). Multiple bands are typically made up of a few anastomosing and interweaving gouge zones. Branches of minor bands occur at the end of the individual deformation bands.

The main mechanism associated with the deformation bands is cataclasis (Figs. 6b–d). The cataclastic zone shows broken and comminuted grains of quartz and feldspar, with some deformed carbonate cement. The intensity of cataclastic deformation is variable and commonly increases with increasing displacement along the zone. Faults with small displacements (less than a few millimetres) show a zone with broken grains and slightly reduced grain size compared with the host rock. Zones with larger displacements commonly show very poor sorting and extremely reduced grain sizes. Such larger faults commonly show one or more thin fracture planes (<0.01 mm thick) cutting through the cataclastically altered grains (Fig. 6c). The occurrence of thin through-going fractures indicates a progression from distributed to more localised shear. The cataclastic zones commonly have a sharp boundary against the undeformed host rock. The calcite cement is strained against the cataclastic zone,

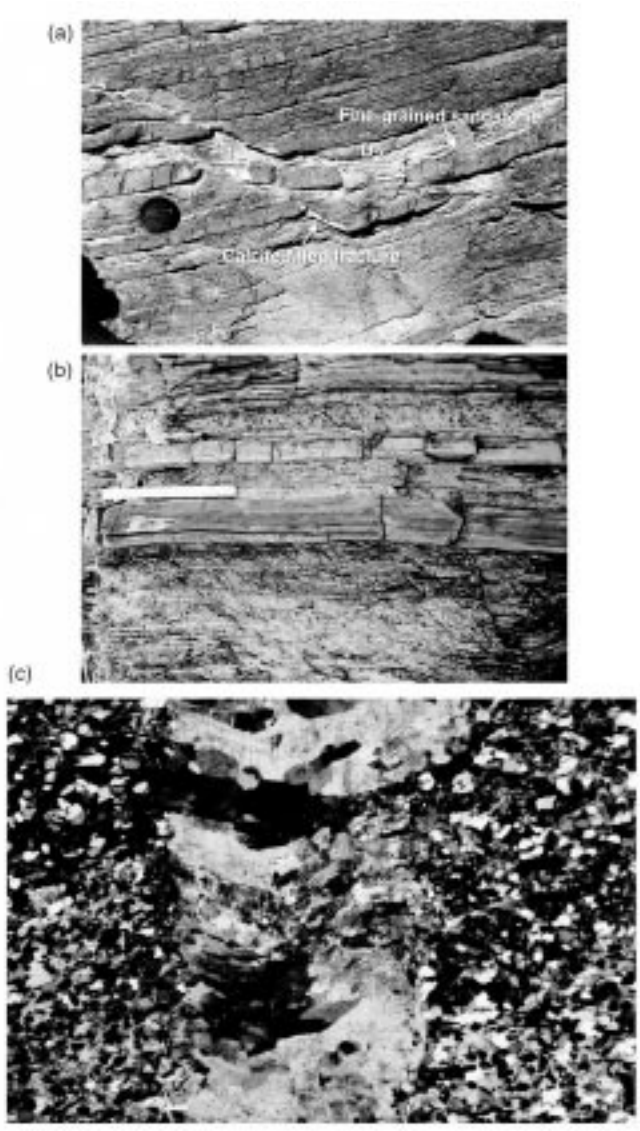

Fig. 7. (a) Fractures cutting carbonate-cemented sandstones interbedded with mudstones. They form pull-aparts (cf. Peacock and Sanderson, 1992) which are filled with calcite. D1 and D2 indicate the displacement geometry which are measured in this study. (b) Fracture styles in the sandstones and mudstones. Note the extension fractures which are limited to sandstone beds and numerous shear fractures in the mudstones which die out at the boundaries to sandstone beds. Length of scale bar is 0.2 m. (c) An extension fracture which is partly filled with fibrous calcite and partly with blocky calcite cement. The width of the picture is 6.25 mm.

suggesting that much of the cement was formed prior to deformation. Calcite cement is observed in some fractures which cut within the cataclastic zones, and indicates that faults were opened and cemented after some shear displacement (Fig. 6d). Polyphase deformation and infill of calcite cement is evidenced by local calcite-filled veins cutting through some cataclastic zones. Compaction or a systematic change in matrix/grain ratio is not observed adjacent to the cataclastic zone in contrast to the fault zones in the more

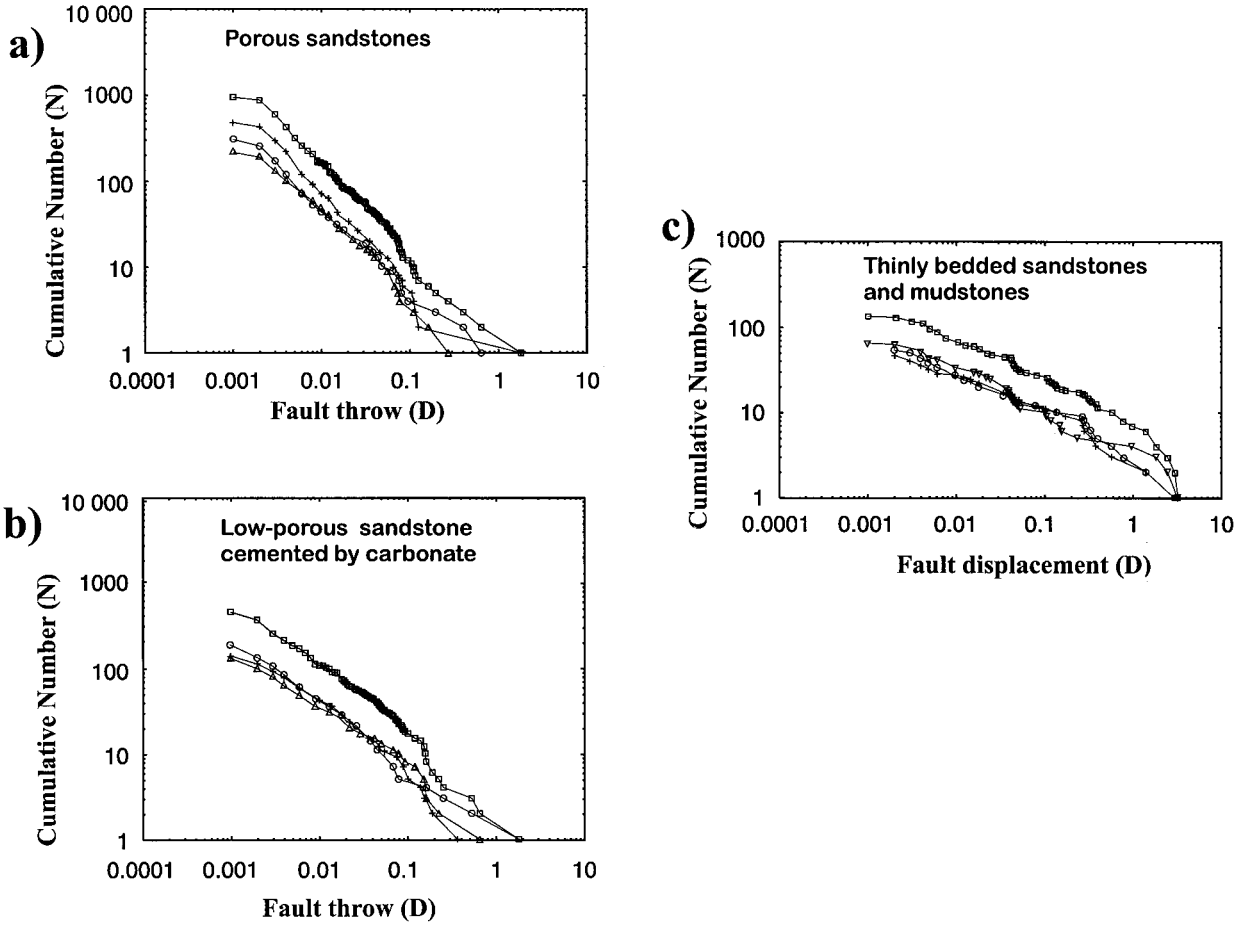

Fig. 8. (a–c) Throw-population of faults in different lithologies plotted on log–log graphs. (a) Faults cutting sandstones with high porosity (10%). Data are derived from three line samples; next to Fault B (circles), around Fault C (crosses) and next to Fault D (triangles). The total dataset is shown by squares. Faults with throws between 2 and 82 mm appear to plot on a straight line, and hence show a power-law relationship. (b) Faults cutting a carbonate-cemented sandstone unit with porosity <4%. The curves represent data from three portions of a line sample; 0–11.5 m (circles), 23.5–34 m (crosses), and 67–95 m (triangles). The total dataset (squares) appears to plot on a straight line for faults with throws between 2 and 92 mm, and a power-law relationship is inferred. (c) Displacement population of faults and pull-aparts cutting thinly bedded carbonate-cemented sandstones and mudstones. Data were collected from a 54 m long traverse along a 26 mm thick sandstone bed (circles), a 43 mm thick sandstone bed (crosses), and a 198 mm thick sandstone bed (triangles). The total dataset was used to analyse a power-law distribution. See text for analysis and interpretation.

porous sandstones (compare Figs. 5b–d and Figs. 6b–d).

Thinly bedded sandstones and siltstones: Tectonic structures in the sandstone beds are dominated by extension fractures and pull-aparts (cf. Peacock and Sanderson, 1992), which were filled with calcite at the time of deformation (Figs. 7a–c). Faults with displacement much less than the sandstone thickness commonly occur as pull-aparts with fibrous grain lineation inclined to the bedding. Typically, these faults refract to lower dips in the adjacent micaceous siltstone, in which tensional movement across the fault plane is less evident. Faults with displacement much larger than sandstone bed thickness (greater than tens of millimetres) show calcite-cemented fault gouges with little evidence of refraction across bedding surfaces and limited extension across the fault plane. Orientation of shear fractures occuring within the micaceous siltstones is very consistent and the mean dip is c. 46°. In the field, distinctions between joints, hybrid fractures and extension fractures cutting these siltstones are difficult because of the general lack of laminae surfaces and the small separation across fractures. Most of the fractures in the siltstones appear to be shear fractures or hybrid shear fractures. Several shear fractures can be traced across bedding surfaces and into extension fractures in sandstone beds, but the majority of the fractures stop at the boundary with the adjacent sandstone bed (Fig. 7b). Layer-parallel faults filled with calcite occur locally in the siltstones and commonly link up the shear fractures to form extensional duplexes.

3. Fault scaling

The location and stratigraphic position of line samples are shown in Figs. 3 and 4(a). The line samples are in the vicinity of major faults and extend through the damage zones, either in hanging wall or footwall or both, and into the less deformed host rock. The fault offset, the dip magnitude, as well as the position of the faults on the transect were measured. Where the transects were oriented oblique to the fault strikes, the position of faults was corrected to $L_1 = L_0/\cos\gamma$, where L_0 is the measured distance between faults striking at the angle, γ, to the sampling line. Lineations on the fault planes have pitch values about 90° (Fig. 4c) and indicate that the dip separation is proportional to the fault throw.

Porous sandstones: Fault offsets were sampled from three transects; (1) in the footwall and next to Fault D, (2) around Fault C, and (3) in the hanging wall and next to Fault B (Fig. 3). These are located in the fine to medium-grained cross-beds of thick sandstone units where offsets down to 1 mm could be measured. More detailed studies in hand specimen and in thin-section reveal more faults with throws less than 2 mm. These faults appear as shear zones with little or no cataclastic deformation. Small fault spacings also limit the counting of fault throws since the reorganization of grains along bands often lead to poorly defined laminae surfaces. Faults with spacing down to 15 mm are commonly included in the datasets. Fault throws up to 1.6 m were recorded but most of them were of the order of a few centimetres or millimetres. Two-hundred and sixteen, 470 and 307 faults were encountered along transects 1, 2 and 3 of 23.4, 56 and 83 m length, respectively. Fig. 8(a) shows the cumulative number, N, of faults with throw greater or equal to D, plotted in a log–log diagram. The datasets suggest that the fault throws have a power-law distribution. The break in the slope at the left end of these curves is due to the under-sampling of small fault throws. The break of the slope at the right end of the slopes is probably caused by the finite sampling length. The latter effect (censoring) was described by Pickering et al. (1995) who introduced a method to compensate this. We have therefore confined a regression analysis to fault throws between 2 and 82 mm, which gives $C = -1.01$, a standard deviation of $C = 0.002$, and a correlation coefficient $r = 0.999$.

Sandstones with low porosity: Sampling from this unit was performed along a $\simeq$95 m long line (285° azimuth) in the hanging wall of Fault A (transect 4 on Fig. 3). The line has two significant breaks (scree deposits) of 22 and 34 m length, respectively. The lengths of the three portions of the line are 11.5, 12.8, and 18.0 m, respectively. Fault offsets were measured along internal laminae surfaces that were weathered to a sharp line against the relatively structureless, medium-grained sandstone bed. Small fault offsets down to $\simeq$2 mm are distinct and can be measured accurately. The number of faults encountered on the three portions of the sampling line were 203, 122 and 134, respectively. A plot of N against D on log scales is shown in Fig. 8(b), where N is the cumulative number of faults with throw greater or equal to D. The total dataset appears to plot on a straight line for the fault throws between 2 and 90 mm. A power-law regression analysis for these data gives a $C = 0.70$, a standard deviation of $C = 0.007$, and $r = 0.998$.

Thinly bedded sandstones and siltstones: Fault data were collected from a cliff section in the hanging wall of Fault A (transect 5 on Fig. 3). Individual sandstone beds persist for several tens of metres away from Fault A. Displacements were measured along the calcite-filled shear fractures in section (Fig. 7a). Many of the faults tend to form pull-aparts and the distinction between extension fractures and pull-aparts becomes difficult when displacements are <5 mm. Population data were obtained in a 54 m long traverse along sandstone beds of 26 ± 2, 43 ± 5 and 198 ± 15 mm thickness. The problem of sampling displacement populations in these sandstones is the low density of shear fractures. Numbers of fault offsets encountered on the lines were only 54, 43 and 69, respectively. Fig. 8(c) shows the cumulative number of faults, N, with fault displacement greater or equal to D. The irregular line defined by these plots reflects the low number of faults encountered in the traverses (covering less than two orders of magnitude). Faults with throws 2 mm and <300 mm appear to plot on a straight line and a power-law regression yields $C = 0.38$, a standard deviation of $C = 0.098$, and $r = 0.978$. Because of the small data set, however, a power-law distribution is questionable.

Because of the limited number of recordings and unknown boundary conditions, power-law functions are often difficult to demonstrate from natural data (e.g. Pickering et al., 1995; Nicol et al., 1996). An estimate of the regression coefficient may vary significantly from one sample to another, simply because the samples are of finite size. To study the influence from finite size sampling, synthetic data were generated from the original data. Random sampling was performed on the total dataset in the porous sandstones with little carbonate cement (Fig. 8a), and the total dataset in the carbonate-cemented sandstones (Fig. 8b). For each of the synthetic datasets, a regression coefficient, C, was calculated. The intervals of regression (i.e. minimum and maximum throw) were equivalent to those used in the analyses in Figs. 8(a) and (b). Fig. 9 shows C plotted against the sample size for 20 random samples of 200, 400, 600 and 800 recordings, respectively. Also shown are the curves of

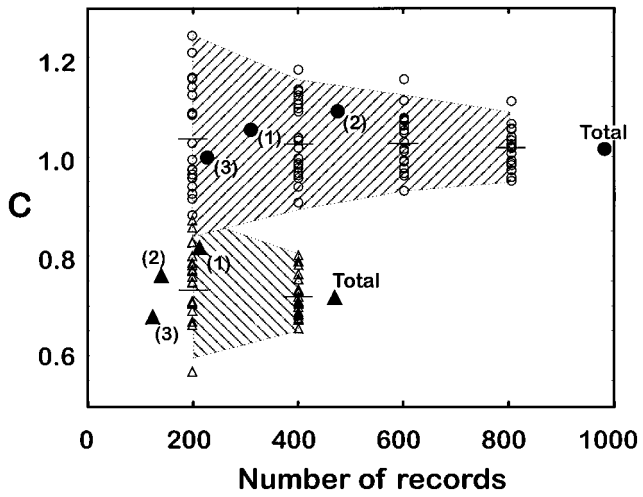

Fig. 9. Plots of calculated *C*-values for samples of variable size. Open symbols represent *C*-values calculated for synthetic random samples derived from the total data samples in porous sandstones (circles) and the low-porous and carbonate-cemented sandstone (triangles). Filled symbols are the *C*-values calculated from the plots in Figs. 8a and 9. The samples are labelled 1, 2 and 3 and refer to the plots shown by circles, crosses, and triangles, respectively, on Fig. 8. The shaded areas cover two times the standard deviation (i.e. 2× standard deviation of *C*-values calculated from 20 random samples). Ninety-five per cent of the cases are expected to fall inside the shaded area assuming a normal distribution of *C*-values.

standard deviation for the *C*-values of random samples, and the *C*-values calculated from the original samples (Figs. 8a and b). As expected, the calculated values of regression coefficients become more widely spread as the size of the sample decreases (e.g. Pickering et al., 1995). On the basis of our statistics, a sample of 200 recordings from the two original datasets could potentially show the same *C*-value. A sample of 400 recordings, however, is expected to show a regression coefficient which can be uniquely ascribed to the original data. We will therefore conclude that the different slopes observed in Figs. 8(a) and (b) reflect a real difference in the scaling relationship of the samples, although the true difference is not known because of the limited sample size in each case.

All transects selected for the different lithologies are located in the damage zones of the major faults (Fig. 3). However, there is a significant distance (<200 m) between these transects and it is possible that the throw populations were influenced by the structural positions at which they were sampled. Both field studies and numerical modelling show that fault linkage during increasing strain will decrease the slope in a $\log N$ vs $\log D$ plot (Wojtal, 1996; Cladouhos and Marrett, 1996). Estimates of the horizontal elongation (i.e. cumulative horizontal separation across fault) along each line indicate some differences in strain magnitudes in the different lithologies. Elongation calculated for the three datasets in the high-porous sandstones were 5.6, 4.0 and 2.4%, respectively. Elongations in the low-porous sandstones were calculated to be 13, 6.0 and 4.8%, respectively. To consider whether the different slope magnitudes observed in Figs. 8(a) and (b) are due to sampling in areas of low and high strain, the cumulative throw across fault per unit distance was calculated. The choice of a regular sampling length is critical, since the variations in strain accounted by the faults may depend on the scale of observation. One example is illustrated in Fig. 10, which shows the spatial distribution of fault throws along line sample 2. The clusters of small faults are not the same at all scales. Small faults are highly concentrated in a 5 m wide zone around the main fault (between 37 and 42 m on the horizontal axis). Outside

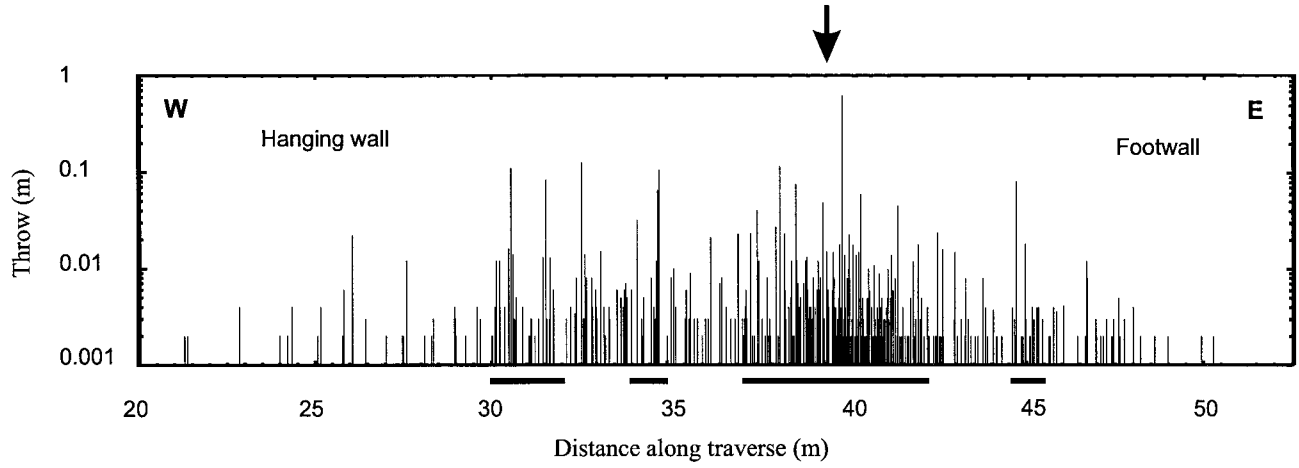

Fig. 10. A histogram showing the throw along individual faults plotted against the distance along line sample 2 (see location in Figs. 3 and 4). The arrow above the histogram indicates the position of the master fault with c. 60 m throw. The thick lines below the histogram show intervals with cumulative fault throws 0.12 m per metre along the line sample. These intervals distinguish high-strain domains from low-strain domains, from which data are plotted in Fig. 12. See text for further description of the sub-sampling.

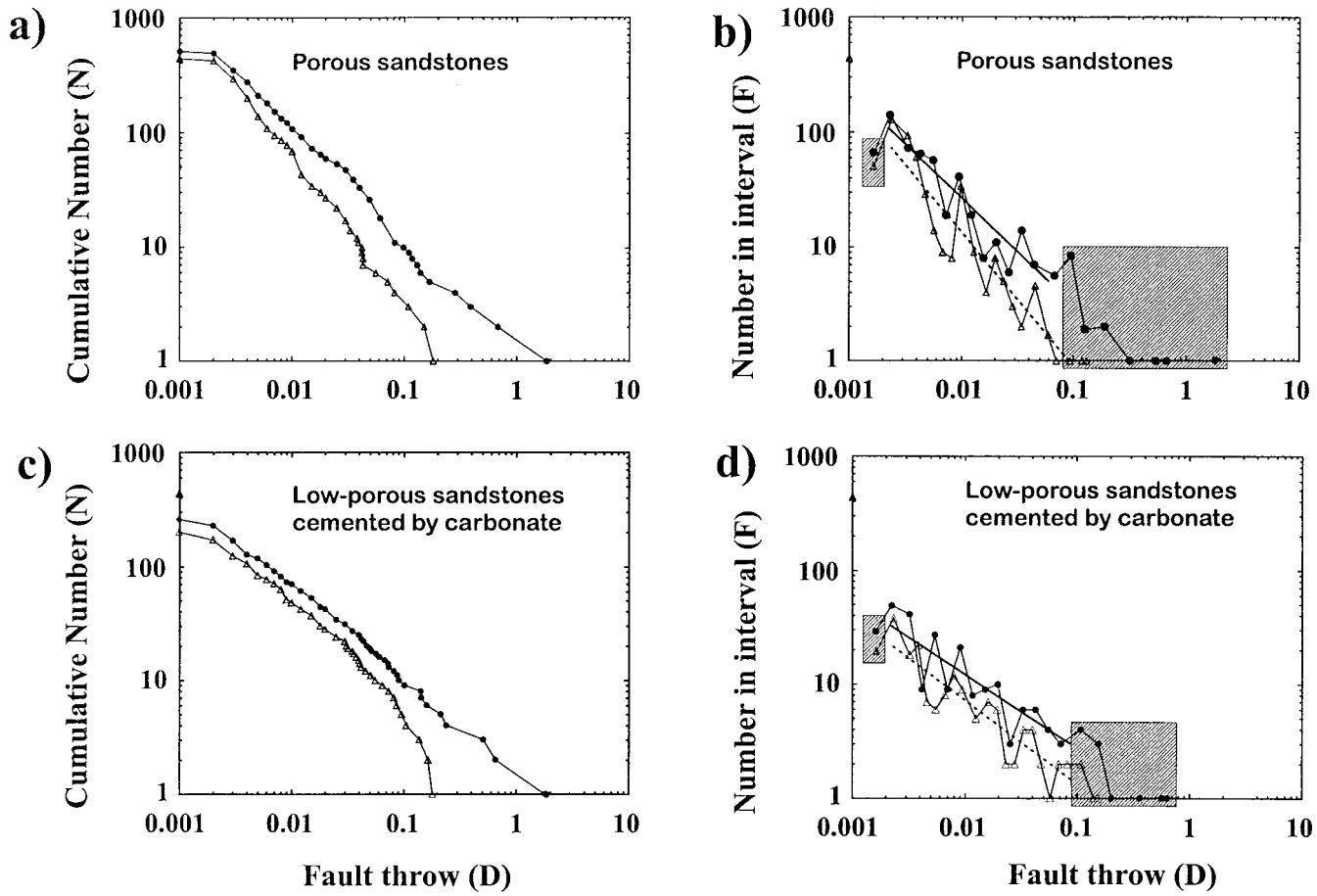

Fig. 11. (a–d) Sub-samples of throw populations plotted on log–log graphs. The original data of the porous sandstones (Fig. 8a) and the low-porous sandstones (Fig. 8b) are subdivided into a high-strain set and a low-strain set. Filled circles: data from high-strain intervals, triangles: data from low-strain intervals. (a) and (b) show the data of the porous sandstones, whilst (c) and (d) show the data of the low-porous and carbonate-cemented sandstones. (a) and (c) show the cumulative number of faults, N, with throw greater or equal to D. (b) and (d) show the number of faults in interval, F, vs fault throw, D. A power-law regression analysis for the data from high-strain intervals and low-strain intervals is shown in (b) and (d). The shaded areas indicate the data which were excluded from this analysis. Dashed line is the slope fitted to low-strain data, whereas the solid line is the slope fitted to the high-strain data. See text and Fig. 10 for sub-sampling procedure and interpretation of data.

this interval, there are minor groups of deformation bands. These groups of bands are often found next to minor slip surfaces with <1 m throw. To see possible effects from fault linkage (cf. Wojtal, 1996), we used sampling intervals of 1 m so the variation in strain next to secondary faults (<2 m throw) could be recorded as well. Typically, the faults next to the master faults and secondary faults were included in a high-strain dataset, whereas the faults in the periphery of these were included in the low-strain dataset. To obtain a relatively high number of faults in the low-strain interval, we set an upper limit of 0.12 m to define the cumulative throw per metre distance in the low-strain interval. Higher values indicated a high-strain interval. The criteria of the present sub-sampling means that the largest fault throws only fall into the high-strain dataset. This sampling bias will strongly affect a log N vs log D plot, where N is the cumulative number of faults with throw greater or equal to D (*cumulative distribution function*). An alternative definition of a power-law distribution is the *discrete frequency of* log D (cf. Pickering et al., 1995), which is expressed as

$$\log F = a_1 - B \log D \tag{2}$$

where F is the frequency of values in an interval of $\log D \pm \delta(\log D)$, D is the measure of size, a_1 is a constant, and B is the exponent. If we have constant log intervals $\delta(\log D)$, the exponent for the *cumulative distribution function*, C in Eq. (1), is consistent with a linear log-interval graph, where $B = C$ (Pickering et al., 1995). The log-interval graph will not be affected by sample biases and can be used as long as the intervals which show the bias are avoided.

The high-strain and low-strain data from both of the sandstones are plotted in Figs. 11(a–d) by using the two methods; *cumulative distribution function* and

the *discrete frequency of* $\log D$. The smallest throw measurement (1 mm) shows truncation, and the largest fault throws (90 mm) are clearly biased by the sub-sampling procedure. Between these values, a regression analysis was performed on the *discrete frequency of* $\log D$ with constant log intervals. Data of the porous sandstones give $C = 0.89$ and 1.13, in the high- and low-strain intervals, respectively (Fig. 11b). The same method gives $C = 0.64$ and 0.73, respectively, for the low-porous sandstones (Fig. 11d). A slightly steeper slope for the low-strain data compared to the high-strain data set could, however, be a finite size effect (fig. 6 in Pickering et al., 1995). The different slopes of the plots could also be ascribed to the sampling technique (e.g. under-sampling of deformation bands in high-strain intervals because of bands occurring side by side below the scale of observation) or to one or several geological processes (e.g. coalescence of deformation bands into groups of bands or slip surfaces, which will decrease the slope in a log N vs log D plot, e.g. Wojtal, 1996). Although such possible factors may play a role, the results shown on Figs. 9 and 11 indicate that the lithology and the associated deformation styles are by far the most important component in describing scaling properties of the small faults.

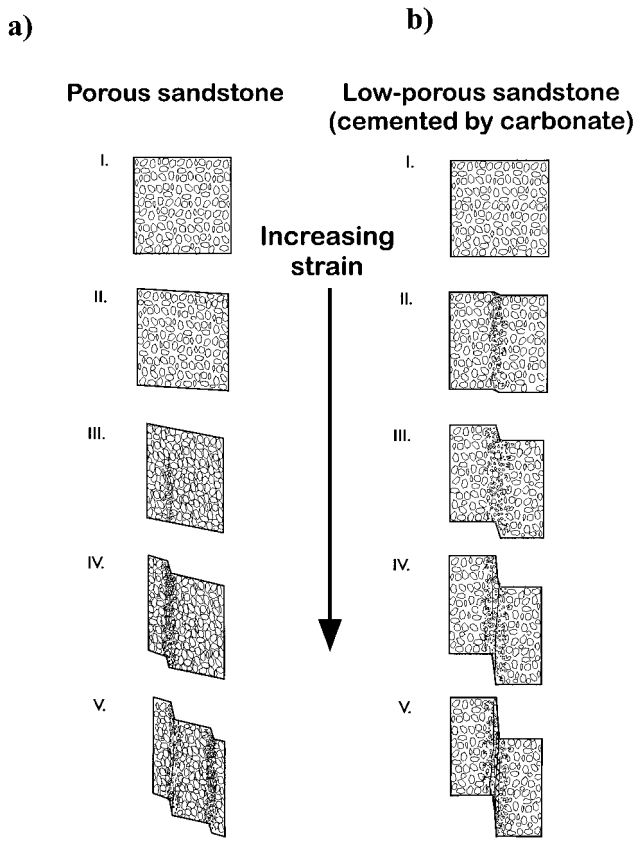

Fig. 12. (a) Model for fault zone formation in the porous and poorly cemented sandstones. (I) Undeformed sediment saturated with pore-fluid. (II) Compaction and particulate flow with no cataclasis. (III) Incipient cataclasis. (IV) Development of a cataclastic zone. (V) Strain-hardening of initial cataclastic zone and formation of a new cataclastic zone. (b) Model for cataclastic deformation and fault development in carbonate-cemented sandstones. (I) Undeformed sandstone. (II) Incipient cataclasis. Grain breakage and cement deformation. (III) Propagation of a cataclastic zone. (IV) Extensive grain deformation and concentration of slip along the cataclastic zone. (V) Slip along thin fracture surfaces and communition of grains. Internal fracture surfaces may be opened and filled by carbonate cement.

4. Deformation mechanisms

This section discusses the deformation mechanisms that are observed in the different lithologies in order to reconstruct the development of the small faults. Microtextural studies indicate that the carbonate-rich sandstones were cemented before fault formation whereas many of the carbonate-poor samples show cementation by carbonate after deformation. Carbonates may cement sandstones at different burial depths and may have a complex cementation history in sandstone matrix as well as in fault zones (Sverdrup and Bjørlykke, 1997). In this section we focus on the different microstructures in the sandstones and try to explain them by comparisons of texture, cement content and timing of cementation relative to deformation.

Deformation mechanisms on the grain scale will vary according to the state of lithification of the sediments (Knipe, 1989). Deformation by grain boundary sliding has been interpreted as taking place in weakly lithified sediments and is enhanced by high pore-fluid pressures (Lucas and Moore, 1986; Knipe, 1989). The grain reorientation and compaction found in fault zones in the carbonate-poor sandstones indicate that these sandstones were incompletely lithified during faulting. Microstructural features indicate that shear movement was caused by grains moving past each other leading to compaction of the movement zone (Fig. 5a). The shear zone geometry also shows that movement was concentrated in one of several localized zones leading to crushing of grains and dramatic reduction in porosity. These features are similar to those described from cores from the lower slope of the Mexican Trench by Lucas and Moore (1986), who assigned them to be of tectonic origin. A sequential development of a fault zone is here proposed from the internal architectures of the faults (Fig. 12a). (I–II) The alignment of elongated grains around faults and at their tip points indicates that the fault zones initiated as shear zones. Because of the low shear strength of the sand, the relative movement of grains led to pore collapse and grain reorganization. (III) Concentration of slip along a discrete zone would take place after some independent particulate flow and compaction. The closer packing of grains will give

greater interlocking of grains and thereby increase the potential for fracturing of individual grains. Thin section studies indicate that the degree of compaction by independent particulate flow can vary widely in the sandstones and seems to depend on the initial porosity (host rock porosity of 15–35% reduced to 5–15% in fault zone). Increasing shear displacement in the compacted portions of the sandstones will lead to grain breakage and, ultimately, a cataclastic zone develops. (IV–V) Further movement could lead to the development of new discrete zones because the existing zone was unable to accommodate further displacement. Cataclastic zones occuring in porous sandstones have been reported widely, and their development is commonly explained by strain-hardening (Aydin and Johnson, 1978; Underhill and Woodcock, 1987). The extreme reduction in porosity and grain interlocking probably increase the cohesion and the frictional coefficient in the zone so that further shear displacement is shifted to the adjacent weaker part of the rock (op. cit.). Further deformation has led to the development of a slip surface, which can carry large displacements. The latter may involve strain-weakening of the deforming rock (Aydin and Johnson, 1978).

Deformation structures in the carbonate-rich sandstones are dominated by through-going cataclastic zones. The sharp boundary between the parent rock and the cataclastic zone which cuts through grains and cement indicates that the sandstones were lithified before deformation. Cement-rich sandstones may deform by cataclasis if the cement strength exceeds the grain strength (Sverdrup and Bjørlykke, 1997). Localization of deformation in the cataclastic zones is documented by the high shear strain measured across them and the preservation of thin lenses of undeformed material in between. Some grains (rock fragments, feldspars) in the undeformed host rock show fractures and cleavage lamellae. Grain splitting at the contact points may then be favoured by the pre-existing weakness planes in grains. The lack of porosity collapse or change in grain/cement ratio towards the cataclastic zone further suggests that the sandstone was well cemented and achieved a considerable strength before deformation. A sequential development of the small faults is outlined on the basis of grain texture and fracture geometries described above (Fig. 12b). (I) Cataclastic deformation at the tip line of faults suggests that the first increment of slip involved grain breakage and cement deformation, and development of a cataclastic zone. (II–III) Further movement probably took place along the existing cataclastic zone leading to greater grain size reduction and probably poorer sorting within the zone. (IV–V) Development of thin fracture planes may decrease the cohesion across the fault zone so that fractures were opened and filled with calcite cement. If the cataclastic zone was strengthened relative to the undeformed rock, new faults could develop beside the older ones. However, the spatial distribution of the small faults does not suggest that strain-hardening was significant for the fault development. The occurrence of solitary faults with several centimetres displacement and the ramified nature of some multiple faults suggest concentration of slip along some faults and development of minor faults to adjust slip along the existing zones. Subsidiary faults may develop to accommodate the space problem around undulating faults, at relay bends, etc. Thus, this mechanism suggests that a fault growing in a strong rock may geometrically harden (cf. Wojtal and Mitra, 1986). This is fundamentally different from a fault growth governed by strain-hardening as suggested for the highly porous and poorly cemented sandstones.

In the bedded sequences with carbonate-cemented sandstones layered with micaceous siltstones the opening mode of fracturing (mode I) is common in addition to shear fracturing (mode II). The exact mechanism for fault development is not fully understood by the authors. Small fault offsets are commonly recorded along pull-aparts which cut at a high angle to bedding. The dihedral angle between conjugate sets in a weak or ductile rock can be larger than the angles expected in a conventional Coulomb material ($\simeq 60^\circ$). Hybrid shear fractures typically have dihedral angles $<60^\circ$ (Hancock, 1985). The faults described here are in some respects similar to pull-aparts described by Peacock and Sanderson (1992), except that numerous shear fractures are visible in the mudstones and seem to stop at the sandstone bed boundary. Under the microscope, there is no evidence for cataclastic deformation along the boundaries of the pull-aparts. Most probably pull-aparts were initiated as tension fractures (mode I). As the fractures propagated into adjacent siltstone, pull-aparts started to form (mode II/III) (fig. 9 in Peacock and Sanderson, 1992). This is further supported by the occurrence of thin tension fractures or joints clustered around faults with several decimetres of displacements. Once an extension fracture is developed, the cohesion is lost until it becomes sealed by the calcite. During this stage, the fracture is the most likely focus for the development of a shear fracture. The shear fractures may propagate into the adjacent siltstone which is weaker and allows for easier propagation of the fault surface.

5. Discussion

5.1. Implications for fault scaling

The suggested fault development discussed above will have implications for describing the scaling behaviour of a fault system as extension proceeds and

minor faults grow into major fault zones. Whether the strain localizes or disperses throughout the rock volume will have considerable effect on log N vs log D plots from an area. A shallow slope on a log N vs log D plot implies that there are few small faults relative to larger faults; a steep slope implies that there are many small faults relative to major faults. The tendency for the porous sandstones to strain-harden implies that new small faults nucleate at a high rate with increasing strain. Mesoscopic small faults will then contribute significantly to the total fault strain. The sandstones with low porosity show less evidence of strain-hardening and, consequently, small faults will contribute less to the total strain. Thus, the steeper slope observed for faults cutting the porous and less cemented sandstones ($C = 1.01$) compared to carbonate-cemented sandstone ($C = 0.70$) can be ascribed to the strain-hardening process in the porous sandstones. Several experiments show that the deformation governed by strain-hardening is typical for porous rocks. Thus, the different deformation mechanisms outlined on Figs. 12(a) and (b) can be relevant for sandstones of other compositions which lithify by various diagenetic processes. However, in generalising these observations to other areas, the influence of rock parameters on the strength and deformational behaviour of the rock needs to be considered. The strength of sandstones is influenced by several factors including external stresses and internal properties such as the porosity, clay content and the degree of cementation (Plumb, 1994). More uncertain to us is how such rock parameters could affect the deformation style of small faults and lead to various scaling parameters of fault systems.

Faulting in the interbedded sandstone and mudstone units seems to be affected by the different mechanical properties of individual beds and the planes of weakness in the mudstones. From the plot on Fig. 8(c), it appears that small fault offsets have a limited contribution to the total extension. In Peacock and Sanderson's (1992) model, preferential slip may take place on existing shear fractures since the strength of siltstone is lower than that of the carbonate-cemented sandstone. Sealing of the existing fractures can be critical if the vein material has a strength which equals or exceeds that of the matrix. Some veins contain blocky calcite cement which indicates that the vein filling was slow relative to the rate of vein opening (cf. Ramsay and Hüber, 1987). If the sealing process was too slow to accommodate the vein opening, the existing fracture represents a plane of weakness which will control the location of subsequent fractures. The one-dimensional density of the shear fractures in the interbedded sandstone and mudstone units is very low (average <1.2 per metre), whereas in the other lithologies this value is 6 per metre. The line samples are in similar structural positions, thus the variable fault intensity can be associated with differences in the deformational style. Because of refraction of faults across siltstone to sandstone boundaries, a true shear fracturing will rarely take place during extension. Fault movement in the sandstone beds is constrained by the slip along the low-angle surfaces in the adjacent siltstones. Extension is therefore accommodated by pull-apart movements and extensional fracturing.

5.2. Implications for fault prediction

Scaling laws have been used to estimate the total extension in sedimentary basins (Walsh et al., 1991) as well as the density of faults that are below the seismic resolution (Needham et al., 1996). Core data have often been integrated in the analysis to justify the use of scaling laws which are inferred from the distribution of the seismically mapped faults. The 'large' faults are commonly obtained from regional lines along well-defined reflectors. North Sea datasets are commonly derived from the Jurassic sandstone reservoirs (Childs et al., 1990; Walsh et al., 1991). Data of the 'small' faults are essentially derived from vertical wells which penetrate heterogeneous rocks in different structural positions with respect to the 'large' faults. In a log $CUMFD$ vs log D plot, where $CUMFD$ is the cumulative fault density and D is the displacement in section, a spread of small-scale fault densities is to be expected because data are collected at different distances from master faults (Fig. 13). However, the present results suggest that lithology also plays a role in the variability of fault densities. Fault densities vary within one and a half orders of magnitude even though every sampling line is located next to a master fault. The scaling behaviour in the variably cemented sandstones described above seems therefore not comparable. The different slopes observed on log N vs log D plots (Figs. 8a–c) suggest that small faults can be subdivided into several displacement populations according to sandstone composition and styles of deformation as they appear on the small scale. This emphasises the importance of distinguishing fracture type (i.e. cataclastic zones, disaggregated zones, dilational zones, etc.) in cores when small faults are compared with seismically mapped faults. It is expected that larger through-going faults which juxtapose the different lithologies can exhibit a different scaling relationship than the faults limited to each lithology type. A change in fault behaviour may occur during the growth of a fault system as deformation bands grow into major slip planes. A scaling relationship between slip planes with several metres throw is, however, not obtained in this study. Strain-weakening is proposed to occur along major slip planes which can carry large displacements (Aydin and Johnson, 1983).

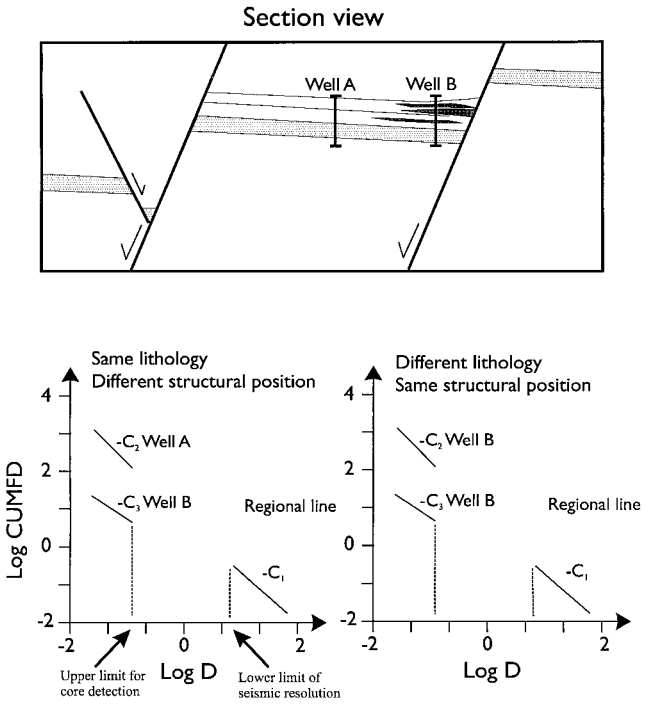

Fig. 13. Schematic diagram showing possible inferences of scaling laws from data of seismically mapped faults and small faults from wells in subsurface basins. A power-law throw distribution may be inferred from each of the datasets but may be uncorrelatable because of the lithological variation and structural position of wells.

The assumption that small and large fault throws follow the same scaling relationship (either power-law or non power-law) is therefore not justified from our study. Small faults sampled from cores are expected to be highly influenced by layering and differing geomechanical properties. This influence is generally little known from subsurface data since there are limited data sampled from each lithology type. Propagation of faults will be disturbed by mechanical boundaries which cause atypical displacement gradients along faults (e.g. Muraoka and Kamata, 1983; Gross et al., 1997). Ideally, small and large faults should be sampled from a geomechanical unit which is thick enough to enclose all the fault samples. This is rarely the case for a fault population covering several orders of magnitude of displacement. Realistic predictions of fault size distributions should therefore consider the presence of 'geomechanical layers' and not rely on uniform scaling relationships. In a geomechanically complex rock the potential for predicting fault geometry and scaling is very reduced and interpretations should be made with caution. However, the understanding of deformational behaviour in relation to mineralogy and grain texture observed in cores can be valuable when the local fault geometry and scaling away from the cores are to be interpreted.

6. Conclusions

Small faults (<0.5 m offset) cutting a heterogeneous rock sequence on Traill Ö, East Greenland, occur with distinctly different geometries. Deformation bands in the high-porous sandstones are subplanar and form zones of subparallel, closely spaced bands. These bands initially deformed by grain boundary sliding which produced folded laminae surfaces and disaggregated zones with tighter grain packing. Porosity in well-sorted sandstones is commonly reduced to 10–15% without any significant cataclastic deformation. Further strain led to grain breakage and development of cataclastic bands. Deformation bands in the low-porous sandstones cemented by carbonate show undulating and interweaving geometries. These bands were formed mainly by cataclastic mechanisms. Concentration of displacement in the cataclastic zones resulted in higher shear strain than those observed in the porous sandstones. Micaceous mudstones with thin interbeds of tight and well cemented sandstones show a strong anisotropy. The sandstones are cut by pull-aparts and extension fractures. Pull-aparts are interpreted to have formed originally as extension fractures and were controlled by the movement along the low-angle shear planes in mudstones (cf. Peacock and Sanderson, 1992).

Fault throw populations presented in this study suggest that the faults in different lithologies exhibit different scaling behaviours. The apparent scaling of fault throws can be linked to the deformation mechanisms inferred from the microstructural studies. Strain-hardening of deformation bands in the high-porous sandstones leads to an increasing number of small faults relative to larger faults compared to small faults in the low-porous sandstones. Pull-aparts in the interbedded sandstone and mudstone show the lowest frequencies and have a smaller proportional contribution to the overall extension than faults of the same size in other lithologies. Extension in these sandstones was also accommodated by extensional fractures. Extensional fracturing may weaken the displacement zone so that slip takes place along some selected pull-aparts. The conclusions drawn here will not exclude the possible influence from fault clustering and fault linkage on scaling behaviour. The local lithology appears to be a major factor that contributes to different scaling parameters of small faults.

Acknowledgements

The field work was financed by Norsk Hydro a.s., Saga Petroleum ASA., and Statoil. Constructive criticism and corrections from David Peacock on an early draft of this paper are greatly acknowledged. We also

thank Ronald Bruhn, John Walsh and Thomas Rage Lerdahl for stimulating a further analysis of the structural data. Reviews by Patience Cowie, Jafar Hadizadeh and Tom Blenkinsop improved the paper significantly. The first author would like to thank Arild Ingebrigtsen for the assistance in the field and help with the development of photographs.

References

Antonellini, M.A., Aydin, A., 1995. Effect of faulting on fluid flow in porous sandstones; geometry and spatial distribution. American Association of Petroleum Geologists Bulletin 79, 642–671.

Antonellini, M.A., Aydin, A., Pollard, D.D., 1994. Microstructure of deformation bands in porous sandstones at Arches National Park, Utah. Journal of Structural Geology 16, 941–959.

Aydin, A., Johnson, A.M., 1978. Development of faults as zones of deformation bands and as slip surfaces in sandstone. Pure and Applied Geophysics 116, 913–930.

Aydin, A., Johnson, A.M., 1983. Analysis of faulting in porous sandstones. Journal of Structural Geology 5, 19–31.

Barton, C.C., La Pointe, P.R., 1995. Fractals in the Earth Sciences. Plenum Press, New York , 265 pp.

Bjørlykke, K., Hø, K., 1997. Effects of burial diagenesis on stresses, compaction and fluid flow in sedimentary basins. Marine and Petroleum Geology 14, 267–276.

Childs, C., Walsh, J.J., Watterson, J., 1990. A method for estimation of the density of fault displacements below the limits of seismic resolution in reservoir formations. In: Buller, A.T. (Ed.), North Sea Oil and Gas Reservoirs II. Graham & Trotman, London, pp. 309–318.

Cladouhos, T.T., Marrett, R., 1996. Are fault growth and linkage models consistent with power-law distributions of fault lengths? Journal of Structural Geology 18, 282–293.

Clemmensen, L.B., 1980a. Triassic rift sedimentation and palaeography of central East Greenland. Grønlands Geologiske Undersøgelse Bulletin 136, 1–72.

Clemmensen, L.B., 1980b. Triassic lithostratigraphy of East Greenland between Scoresby Sund and Kejser Franz Josephs Fjord. Grønlands Geologiske Undersøgelse Bulletin 139, 1–56.

Cowie, P., Scholz, C., 1992. Displacement–length scaling relationships for faults: data synthesis and discussion. Journal of Structural Geology 14, 1149–1156.

Cowie, P., Knipe, R.J., Main, I.G., 1996. Introduction to the Special Issue. Journal of Structural Geology 18, v–xi.

Gross, M.R., Gutiérrez-Alonso, G., Bai, T., Wacker, M.A., Collinsworth, K.B., Behl, R.J., 1997. Influence of mechanical stratigraphy and kinematics on fault scaling relations. Journal of Structural Geology 19, 171–183.

Hancock, P.L., 1985. Brittle microtectonics: principles and practice. Journal of Structural Geology 7, 437–457.

Jamison, W.R., Stearns, D.W., 1982. Tectonic deformation of Wingate Sandstone, Colorado National Monument. American Association of Petroleum Geologists 66, 2584–2608.

Knipe, R.J., 1989. Deformation mechanisms; recognition from natural tectonites. Journal of Structural Geology 11, 127–146.

Lucas, S.E., Moore, J.C., 1986. Cataclastic deformation in accretionary wedges: Deep Sea Drilling Project Leg 66, southern Mexico, and on-land examples from Barbados and Kodiak Islands. In: Moore, J.C. (Ed.), Structural Fabrics in Deep Sea Drilling Projects Cores from Forearcs. Geological Society of America Memoir 166, pp. 89–104.

Muraoka, H., Kamata, H., 1983. Displacement distribution along minor fault traces. Journal of Structural Geology 13, 483–495.

Needham, T., Yielding, G., Fox, R., 1996. Sampling of fault populations using sub-surface data: a review. Journal of Structural Geology 18, 135–147.

Nicol, A., Walsh, J.J., Watterson, J., Gillespie, P.A., 1996. Fault size distributions—are they really power-law. Journal of Structural Geology 18, 191–197.

Peacock, D., Sanderson, D.J., 1992. Effects of layering and anisotropy on fault geometry. Journal of Geological Society London 149, 793–802.

Pickering, G., Bull, J.M., Sanderson, D.J., 1995. Sampling power-law distributions. Tectonophysics 248, 1–20.

Plumb, R.A., 1994. Influence of composition and texture on the failure properties of clastic rocks. In: Rock Mechanics in Petroleum Engineering, Proceedings Volume for the Second SPE/ISRM Rock Mechanics Conference, 29&31 August 1994, pp. 13–20.

Price, S.P., Whitham, A.G., 1997. Exhumed hydrocarbon traps in East Greenland: Analog for the Lower–Middle Jurassic play of Northwest Europe. American Association of Petroleum Geologists Bulletin 81, 196–221.

Ramsay, J., Huber, M.I., 1987. The Techniques of Modern Structural Geology. Volume 2: Folds and Fractures. Academic Press, London.

Surlyk, F., 1991. Sequence stratigraphy of the Jurassic–lowermost Cretaceous of East Greenland. American Association of Petroleum Geologists Bulletin 75, 1468–1488.

Surlyk, F., Clemmensen, L.B., Larsen, H.C., 1981. Post-Paleozoic evolution of the East-Greenland continental margin. Canadian Petroleum Association Memoir 7, 611–645.

Sverdrup, E., Bjørlykke, K., 1997. Fault properties and development of cemented fault zones in sedimentary basins. Field examples and predictive models. In: Møller-Pedersen, P., Koestler, A.G. (Eds.), Hydrocarbon Seal, Importance for Exploration and Production. Norwegian Petroleum Society Special Publication 7, pp. 91–106.

Underhill, J.R., Woodcock, N.H., 1987. Faulting mechanisms in high-porosity sandstones; New Red Sandstone, Arran, Scotland. In: Jones, M.E., Preston, R.M.F. (Eds.), Deformation of Sediments and Sedimentary Rocks. Geological Society of London Special Publication 29, pp. 91–105.

Upton, B.G.J., Emeleus, C.H., Rex, D.C., Thirlwall, M.F., 1995. Early Tertiary magmatism in NE Greenland. Journal of the Geological Society of London 152, 959–964.

Walsh, J.J., Watterson, J., Yielding, G., 1991. The importance of small-scale faulting in regional extension. Nature 351, 391–393.

Wojtal, S.F., 1996. Changes in fault displacement populations correlated to linkage between faults. Journal of Structural Geology 18, 265–279.

Wojtal, S.F., Mitra, G., 1986. Strain hardening and strain softening in fault zones from foreland thrusts. Geological Society of America Bulletin 97, 674–687.